

Angular Distortions at Benzylic Carbons Due to Intramolecular Polarization-Induced Metal–Arene Interactions: A Case Study with Open-Shell Chromium(II) NHC Complexes

Andreas A. Danopoulos,^{*,†} Kirill Yu. Monakhov,[†] Vincent Robert,^{*,‡} Pierre Braunstein,^{*,†} Roberto Pattacini,[†] Susana Conde-Guadaño,[§] Martin Hanton,[§] and Robert P. Tooze[§]

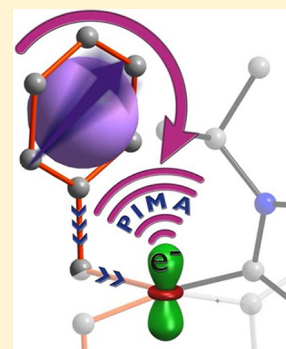
[†]Laboratoire de Chimie de Coordination, Institut de Chimie (UMR 7177 CNRS), Université de Strasbourg, 4 Rue Blaise Pascal, 67081 Strasbourg, France

[‡]Laboratoire de Chimie Quantique, Institut de Chimie (UMR 7177 CNRS), Université de Strasbourg, 1 Rue Blaise Pascal, 67008 Strasbourg, France

[§]Sasol Technology UK Ltd, Purdie Building, North Haugh, St Andrews, Fife, U.K. KY16 9ST

Supporting Information

ABSTRACT: The synthesis and full characterization of the unprecedented open-shell Cr(II) benzyl organometallic complexes $[\text{Cr}(\text{NHC})_2(\text{benzyl})_2]$ (**2**) and $[\text{Cr}(\text{NHC}^*)(\text{benzyl})_2]$ (**3**) (NHC = *N,N'*-diisopropylimidazol-2-ylidene; NHC* = *N,N'*-bis(2,6-diisopropylphenyl)imidazol-2-ylidene) from $[\text{Cr}(\text{benzyl})_3(\text{THF})_3]$ and $[\text{CrCl}_2(\text{THF})_2]/[\text{Mg}(\text{benzyl})_2]$, respectively, uncovered unusually acute angles (93° in **2** and 76° in **3**) at the sp^3 benzylic C of the coordinated benzyl ligands. Detailed theoretical analyses (DFT and CASPT2) of the four- and three-coordinate Cr(II) species were performed to elucidate the physical origin of the benzyl bending and led to the recognition of a noncovalent, intramolecular polarization-induced metal–arene (PIMA) interaction as being responsible for it. The energetic contribution from a single PIMA interaction is estimated to be ca. 50 kJ/mol. A comparison with the origin of the angular distortions in the d^0 $[\text{Zr}(\text{benzyl})_4]$ complex will also be presented. Sharing the common origin of an induced-dipole charge density scheme with intermolecular anion– π interactions, the intramolecular PIMA interaction concept involving a transition metal unpaired d electron and arene– π orbitals can be viewed as an extension of intermolecular anion– π interactions and leads to remarkable quantitative prediction of the observed structural distortions. PIMA interactions may manifest themselves in diverse structural and dynamic phenomena and have broad implications in chemical sciences.



INTRODUCTION

Studies on intermolecular noncovalent interactions and their role in chemical and biological phenomena are of considerable current interest, owing to their relevance to molecular recognition, self-assembly, transport, organocatalysis, sensors, and crystal engineering. A better understanding of the intermolecular interactions involving polarizable π networks has been gained through multidimensional experimental and theoretical work on model systems, including accurate structural determinations by crystallography and predictions by high-level computational methods.¹

Noncovalent interactions fall in the range of ca. 1–50 kJ/mol and extend beyond ca. 3.0 Å, where conventional chemical bonding is absent.¹ At shorter distances, they may still be present but masked by the much stronger covalent bonding. Currently, the arene–arene and cation– π noncovalent interactions are the best understood, the latter being common in nature due to the favorable interaction of electron-rich domains with neighboring positive charges. Very recently, rapid progress has occurred on intermolecular perfluoroarene– π , H-bond– π , and anion– π interactions, π denoting an aromatic ring system.^{2,3} The interaction between the induced instantaneous

dipole in a π system and a negative charge is the origin of these rather counterintuitive attractive polarization forces.^{1,4} Model systems in which specific intramolecular, noncovalent forces can be singled out and correlated to observed macroscopic features are highly desirable and could lead to new fundamental and applied knowledge.

Access to new, well-defined chromium organometallics relevant to the industrially and academically important homogeneous and heterogeneous oligomerization and polymerization of ethylene^{5–8} has generated considerable interest, and in this context, we targeted N-heterocyclic carbene (NHC)-stabilized complexes in order to take advantage of the unique and tunable stereoelectronic properties of the NHC ligand. Importantly, NHC ligands are of increasing interest with a broad range of applications.^{9–11} Furthermore, unique activities and selectivities have been reported for Cr-based catalysts^{12,13} and Cr–arene π interactions may play a more significant role during catalysis than previously thought.¹⁴

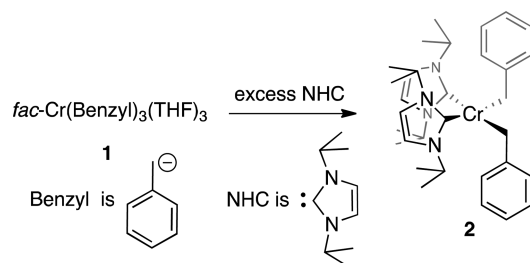
Received: December 27, 2012

Herein, we describe novel open-shell benzyl Cr^{II} organometallics in which remarkable angular distortions at the Cr–CH₂–Ph sp³ carbon are observed. Although the benzyl ligand is well known for its ability to interact with electron-deficient metal centers through its π -aromatic system,¹⁵ possibly leading to rather acute angles at their sp³ benzylic carbon, it will be demonstrated here, using high-level computational methods, that this explanation does not provide sufficient insight in our case. We will also compare the bending of the benzyl ligands in the new d⁴ Cr^{II} organometallics [Cr(NHC)₂(benzyl)₂] (2) and [Cr(NHC*)(benzyl)₂] (3) (NHC = *N,N'*-diisopropylimidazol-2-ylidene; NHC* = *N,N'*-bis(2,6-diisopropylphenyl)imidazol-2-ylidene) with that in the d⁰ [Zr(benzyl)₄] complex, which exists in two polymorphic structures with different metrical data, in particular for the benzyl ligands; this has been recently revisited using DFT methodologies.¹⁶ The involvement of intramolecular noncovalent interactions in the Cr^{II} complexes and the role of polarization effects will be justified. To the best of our knowledge, the contribution of the latter to the bonding of open-shell transition metal arene complexes has previously not been recognized. We anticipate that the study of their nature, range, scope, and creative manipulation may complement established paradigms on structure/bonding relationships and have unforeseeable implications in open-shell transition metal chemistry. This also opens the possibility that in other cases, too, a new insight into the reasons for structural distortions may be required.

RESULTS AND DISCUSSION

Initial attempts showed that complex 2, a N-heterocyclic carbene-stabilized 3d⁴-Cr^{II} bis-benzyl complex, is accessible from the Cr^{III} organometallic complex 1 (for structural details, see Table S1 and Figure S2 in the Supporting Information (SI))¹⁷ by a redox reaction that is not yet fully elucidated (Scheme 1).

Scheme 1. Synthesis of [Cr(NHC)₂(benzyl)₂] (2) in 2·THF



Complex 2 has limited thermal stability at room temperature and was characterized by chemical and X-ray diffraction methods (Table S1, SI). The metal coordination geometry in 2 is distorted square-planar (Figure 1), with an unusual *cis*-arrangement of the benzyl ligands.

Noticeably, all ligands in this 12-valence electron complex are strong carbon σ -donors. Although bond lengths are in the expected ranges, the values of the bond angles subtended at the benzylic carbons (hereafter referred to as *critical angles*) are remarkable: 100.79(11)° for Cr1–C26–C27 and 93.11(13)° and 93.18(19)° for Cr1–C19–C20; the latter two values correspond to the benzyl ligand that is disordered over two positions, A and B, respectively.

A statistical analysis of transition metal benzyl angles found in the CSD is provided in Figure S1 (SI). It shows that in the

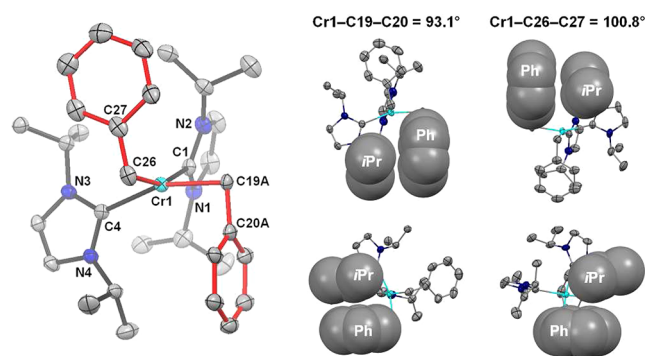


Figure 1. (Left) ORTEP of the Cr^{II} benzyl complex 2 in 2·THF. Ellipsoids are at the 40% probability level; only one disordered benzyl group *trans* to atom C4 is shown. Hydrogen atoms are omitted for clarity. Selected distances (Å) and angles (deg): Cr1–C4 2.1624(15), Cr1–C1 2.1668(16), Cr1–C19A 2.153(3), Cr1...C20A 2.684(3), Cr1–C26 2.1849(16), Cr1...C27 2.854(2); C4–Cr1–C1 90.76(6), C4–Cr1–C26 93.59(6), C1–Cr1–C26 158.70(6), C27–C26–Cr1 100.79(11), C20A–C19A–Cr1 93.11(13) C20B–C19B–Cr1 93.18(19). (Right) Partial space-filling representation of the experimental structure, involving the arene ring of the benzyl and the *iPr* group of the corresponding NHC ligand, indicating the absence of interligand intramolecular contacts.

majority of the examples, the M–CH₂–C_{ipso} angle lies in the 110–120° range, intuitively corresponding to a classical η^1 arrangement implying an sp³ hybridization for the metalated carbon. There is a gradual (apparently not bimodal) shift toward more acute angles, suggesting a flat energy profile responsible for the decrease of M–CH₂–C_{ipso}.

Remarkably, structurally characterized Cr benzyl (C₆H₅CH₂[−], Bz) complexes are relatively rare (26 hits in the CSD, including 4 for Cr^{II}, 20 for Cr^{III}, and 2 for Cr^{VI}), despite the important role of this ligand in the development of stable transition metal organometallics¹⁸ and, consequently, its widespread use in group 4 metal model compounds (e.g., [MBz₄], M = Ti, Zr, Hf) and in catalytic precursors.^{19,20}

Only twice before have angular distortions comparable to those in 2 been observed in Cr chemistry: (i) in the Cr^{VI} complex [Cr(*Nt*Bu)₂Bz₂] and the related [Cr(κ^2 -NCMe₂CH₂CH₂CMe₂N)Bz₂]²¹ and (ii) the diamagnetic Cr^{II} nitrosyl complex [Cr(NO)(*NiPr*)₂Bz₂].²² However, their origin has not been investigated in detail. When acute (<109°) critical angles are observed in group 4 and 5 organometallics, two widely accepted rationalizations are offered. The first invokes the role of intermolecular crystal packing forces. However, in the structure of 2·THF, there are no specific intermolecular contacts involving the benzyl ligands, neither with the solvent of crystallization nor with neighboring molecules (Figure 2).

The second rationalization postulates overlap between the empty metal d orbitals and filled π orbitals of the aromatic ring, in particular the one mostly localized on the aromatic *ipso* carbon (see also further discussion below) and has been applied to d⁰ [MBz₄] (M = Ti, Zr, Hf) complexes.²³ However, in 2·THF the *d*_{ipso} values (Cr–C27 2.854(2) Å, Cr–C20A 2.684(3) Å, and Cr–C20B 2.747(3) Å) are at least 30% larger than the *d*_{benzyl} (Cr–C26 2.185(2) Å, Cr–C19A 2.153(3) Å, and Cr–C19B 2.232(4) Å) (Scheme 2), so that an explanation restricted to orbital overlaps appears insufficient and we suspected that other factors may be at work.

The high-level theoretical calculations detailed below show that electrons localized in d orbitals switch on polarization

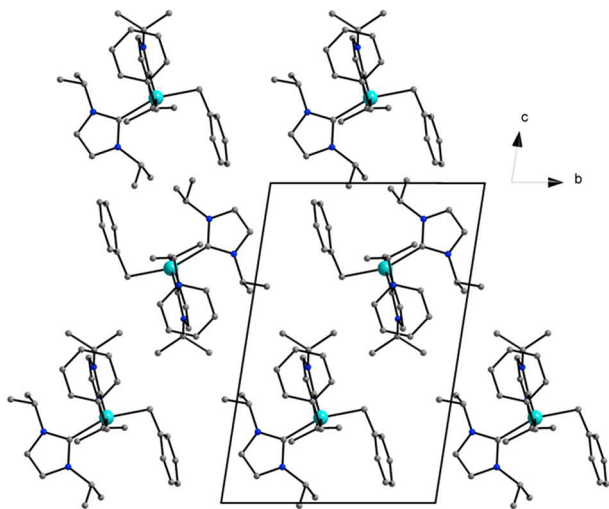
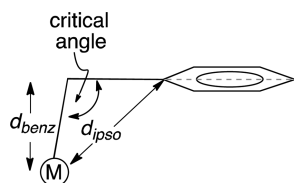


Figure 2. Packing in the crystal structure of 2·THF showing the absence of specific intermolecular interactions.

Scheme 2. Relevant Geometrical Parameters in Metal Benzyl Systems



forces, leading to a type of interaction, namely, polarization-induced metal–arene (PIMA) interaction, that has previously not been identified in transition metal chemistry (Figure 3).

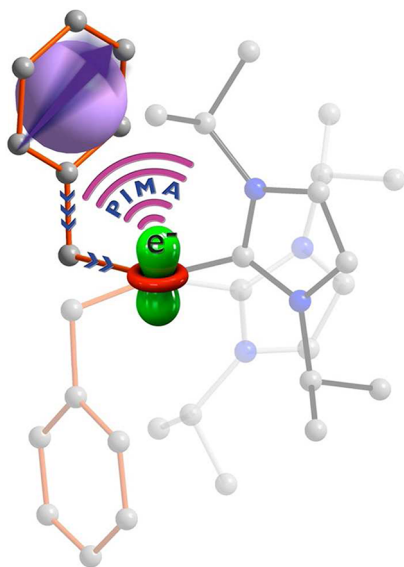


Figure 3. Schematic representation of intramolecular polarization-induced metal–arene (PIMA) interactions (purple arcs) between a single electron in a d orbital and the aromatic benzylic system, resulting in an acute critical angle at the benzylic C atoms in 2. The arrow along the $C_{\text{ippo}}-C_{\text{benzylic}}$ and $C_{\text{benzylic}}-Cr$ bonds indicates electron-withdrawing effects due to the Cr^{II} cation; the arrow across the aromatic ring represents the instantaneous dipole responsible for the noncovalent interactions.

Very recently, polarization-induced lone-pair–arene interactions were briefly outlined in main group chemistry for $As(\text{III})-\pi_{\text{arene}}$ complexes.²⁴ However full elucidation of this phenomenon was not provided, and the conclusions made were based only on the data obtained from the use of density functional theory and Hartree–Fock (HF) calculations that do not deal with polarization effects. Herein, we combine *ab initio* and density functional theory (DFT) methods to delineate the role and mode of action of the PIMA and its structural consequences.

Full (nonconstrained) gas-phase geometry optimizations of 2 were carried out for the $S = 0, 1,$ and 2 spin states using relativistic non- and dispersion-corrected^{25–29} DFT at ZORA-UBP86(-D3)/TZP and established a quintet ($S = 2$) ground-state structure, referred to as 2_{comput} (see Tables S2 and S3, SI). The other spin states are too high in energy (ca. 0.7 eV for $S = 1$) to compete with the $S = 2$ state. Environment continuum medium effects modeling the situation in solution were also considered (see Table S4, SI). For both the gas-phase and the solvent shell situations, the experimental geometry was reproduced satisfactorily enough (as detailed below) to suggest that specific intermolecular crystal packing forces are negligible.

To evaluate the possible impact of London dispersion forces on the benzylic angles in 2_{comput} , we performed constrained geometry optimizations of the target complex for its $S = 2$ ground state, with and without dispersion correction. The relevant potential energy surfaces (PESs) were obtained and are illustrated in Figure 4. They show the change in the total

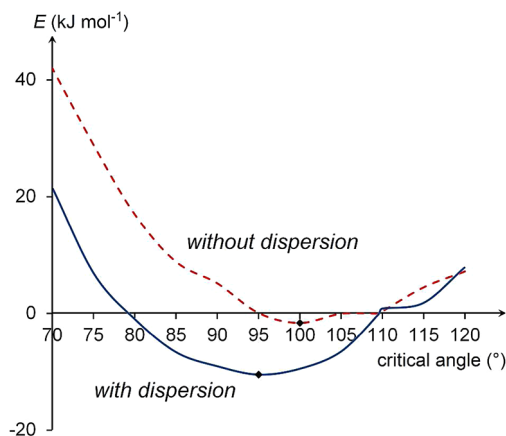


Figure 4. Potential energy surfaces (PESs) obtained from the critical angle constrained geometry optimizations of 2_{comput} with and without Grimme's dispersion correction of D3 generation to the UB86 functional. The black rhombuses indicate the energy minima on the PESs.

energy of the system as a function of one critical angle, the value of which was varied in the range $70-120^\circ$, while the geometry of the molecule was optimized. By fixing a benzyl angle at 100.0° , which corresponds to the energy minimum on the potential energy surface without applying dispersion corrections (UB86), we find the optimized angle of the other benzyl ligand at 102.0° . By fixing now a benzyl angle at 95.0° , which corresponds to an energy minimum for the constrained geometry of 2_{comput} when taking into account dispersion corrections (UB86-D3), we find a value of 93.1° for the angle of the other benzyl ligand. However, the reasons for differentiation observed experimentally in 2·THF between the two benzyl angles (ca. 93° and 101°) remains unclear. This

feature may be the result of the competition between the PIMA interaction discussed in this work and the steric repulsion that would result from the simultaneous bending of two benzyl ligands, and this is the subject of work in progress. The low-angle value-regime experimentally observed and supported by DFT calculations including dispersion forces remains intriguing.

Thus, we wanted to explore in more detail the possible physical reasons that may contribute to the bending of these benzylic critical angles and analyze the relevant intramolecular interactions in **2**, using a wave function-based CASPT2 strategy that is also more suitable for open-shell electronic structures and when weak interactions are simultaneously present.³⁰ On the basis of the additivity of the energy corrections inherent in a perturbative scheme, we explored the polarization effects involving the aromatic rings (see SI). A CAS[10,10] active space was first converged onto the benzyl ring π network (6 electrons, 6 MOs) together with the four relevant d-type orbitals (4 electrons, 4 MOs). These CAS[10,10]SCF calculations were performed as a function of the critical angle to evaluate the contributions arising from (i) the interaction between the Cr d orbitals and the C_{ipso} orbital and (ii) the fluctuating induced dipole within the π system depicted by six MOs (Figure 5). The latter contribution evidently cannot be accounted for using a classical electrostatic description. We show below that the dominant contribution to PIMA arises from a polarization of the benzylic π system induced by the metal d shell rather than by the cationic nature of the soft metal center.

A leading open-shell character for all spin states (even for $S = 0$) was observed, meaning that the mostly d-like MOs are essentially singly occupied. Quantitatively, the analysis of the wave functions led to natural 3d-type orbitals with occupancy numbers in the range 0.999–1.001. Subsequently, the active space was reduced to a minimal CAS[4,4] consisting of the four singly occupied d-type orbitals, and a perturbative treatment (CASPT2) was carried out by (i) freezing the benzyl π network, (ii) allowing the π back-donation, and (iii) including all the active and inactive MOs. This was done in order to capture the PIMA energetic contribution and its role in the dictation of the observed geometry. The potential energy curve displays a minimum at ca. 103° in the absence of charge fluctuations within the benzyl ring (Figure 6, top). A similar observation is made when π back-donation is switched on. Thus, the origin of the smaller critical angle values (ca. 93.1°) found experimentally cannot be solely attributed to the direct interaction between the Cr d and C_{ipso} orbitals.

Indeed, as soon as the polarization effects of the benzyl ring are included, the minimum is shifted down to ca. 93° , supporting the herein proposed role of this polarization-induced mechanism. Using as reference the total energy corresponding to a critical angle value of 109.5° , we also calculated an *energy stabilization* of ca. 23 kJ/mol, as compared to 5 kJ/mol in the absence of PIMA interaction (see Figure 6, top). Not only is the experimental structure well reproduced, but the calculated critical angle value is in excellent agreement with the value of the most acute angle extracted from our reference and most accurate CAS[10,10]PT2 calculations (ca. 93° in Figure 6, bottom).

The behavior of the energy associated with the fluctuating induced dipole (see π -like MOs in Figure 5) interacting with the singly occupied Cr 3d-character MOs is monotonic, and a significant energy gain arising from the PIMA interaction of ca.

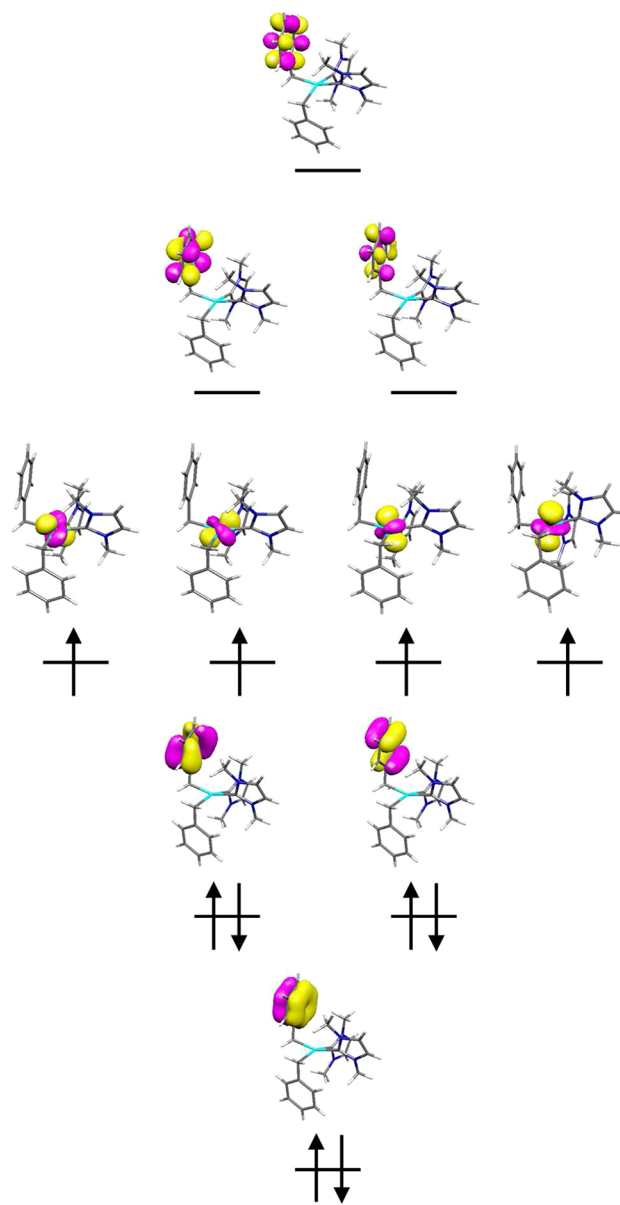


Figure 5. CASSCF active MOs of **2** and their occupancies corresponding to the electronic configuration in the $S = 2$ spin state.

40 kJ/mol is calculated when the angle is changed from 109.5° to 90° (see Figure 6, bottom).

The scope and relative importance of PIMA in the presence of other intramolecular interactions (covalent or not) in organometallics were the next key questions to address. Bearing in mind that the occurrence of PIMA requires (i) occupancy of a d orbital suitably oriented with respect to the aromatic ring (see Figure 5) and (ii) the presence of an electron-withdrawing moiety (the role fulfilled by Cr(II) in **2**), we examined how depletion of electron density on the metal center may influence the magnitude of the “critical angle”, first by maintaining the same 3d orbital occupancy and second by moving to a d^0 situation. In the former case, the structural impact of removal of a NHC ligand from **2**, leading to a hypothetical three-coordinate Cr(NHC)(benzyl)₂ complex, **2'**_{comput} was theoretically investigated. DFT full and constrained structure optimization carried out at the UB973-D3 level of theory led to a geometry displaying one critical angle value of 76.3°

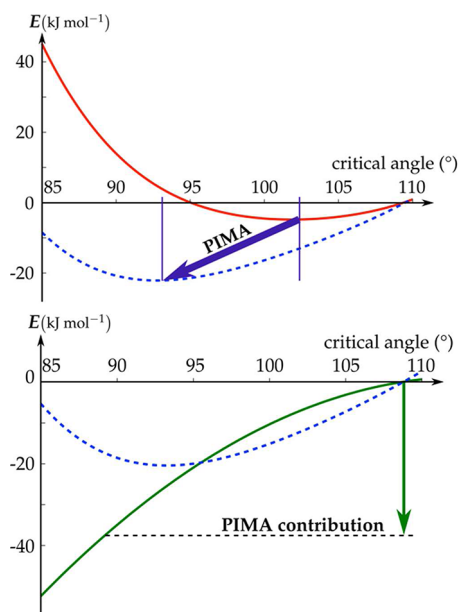


Figure 6. (Top) Dashed blue and solid red curves represent the CAS[4,4]PT2 total energies (in eV) with inclusion and exclusion of the PIMA interaction, respectively. The reference energies are taken for a critical angle value of 109.5° (i.e., sp^3 geometry). (Bottom) Dashed blue curve represents the CAS[10,10]PT2 potential energy curve (in eV) of the $S = 2$ ground state of **2** as a function of the critical angle (deg). A similar curve holds for $S = 0, 1$. A minimum occurs for 93° , a value observed in the crystal structure. The solid, green curve represents the variation of the PIMA interaction as a function of the critical angle.

(Figure 7; 78.2° at UBP86 and Figure S6 in SI) for a $S = 2$ ground state, which made the synthesis of such a complex particularly appealing and worthwhile.

Although a three-coordinate complex of the type $[\text{Cr}(\text{NHC})(\text{benzyl})_2]$ is expected to be less stable than a four-coordinate $[\text{Cr}(\text{NHC})_2(\text{benzyl})_2]$ complex and to exhibit a smaller ligand field (cf. the energy splitting parameters Δ' and Δ , respectively, given in Figure 7), three-coordinate complex **3** was obtained by using a carbene ligand with a larger buried volume³¹ (Scheme 3). The latter is a unique example of a three-coordinate Cr^{II} complex with carbon-only donor ligands. This complex was fully characterized by spectroscopic and diffraction methods (see Figure 8 and Table S1 in SI).

In remarkable agreement with $2'_{\text{comput}}$ complex **3** exhibits a Cr center coordinated by one NHC and two benzyl groups and shows the predicted geometrical features, i.e., a distorted trigonal planar environment (sum of the angles at Cr 358.1°) and critical angles at C28 and C35 of $97.9(2)^\circ$ and $76.6(2)^\circ$, respectively. The occurrence of such an extreme bending was inspected following the same energy partitioning as for **2**. A comparative summary of the changes in the critical angle values for **2** and **3** is given in Table 1.

The operation of an instantaneous dipole in the arene ring is responsible for a reduction of the critical angle value by ca. 10° with respect to a static picture, leading ultimately to the experimental values. The gain of 68 kJ/mol due to the PIMA is an underlying factor for the stabilization of **3** and may be responsible for its isolability.

As mentioned above, we examined the effect of a complete depletion of the d electron density in the vicinity of the aromatic ring. This should reduce the PIMA contributions and

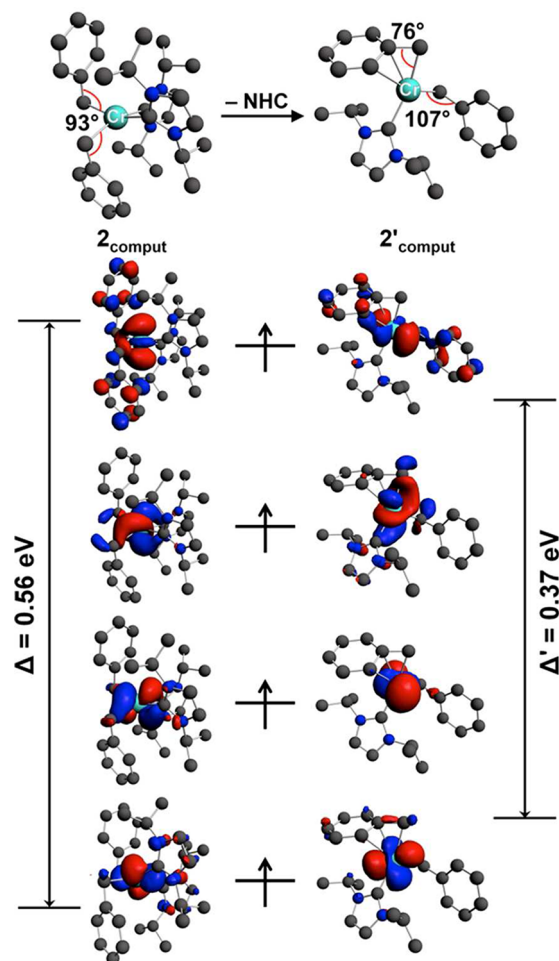
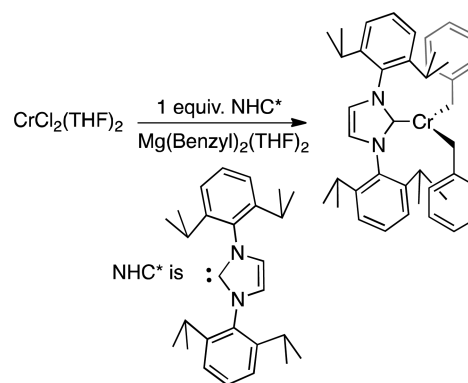


Figure 7. Spatial representation of the four highest singly occupied DFT-generated α -spin MOs with dominant Cr d-type character of the Cr^{II} benzyl complexes 2_{comput} (left) and $2'_{\text{comput}}$ (right) in their ground states, $S = 2$. Hydrogen atoms are omitted for clarity.

Scheme 3. Synthesis of Three-Coordinate Complex **3**



result in larger benzylic critical angles. Indeed, this was observed when the $4d^0$ complex $[\text{ZrBz}_4]$ was subjected to an analysis similar to those described for **2** and **3**. For the same change of the critical angle from 109.5° to 90° , the PIMA contributions vary by only ca. 10 kJ/mol (versus 40 and 55 kJ/mol for **2** and **3**, respectively), as anticipated. This establishes that in general, and in particular with softer metal ions, the cation-induced polarization of the benzyl π system could at best be a minor contribution to PIMA. The acute critical angles

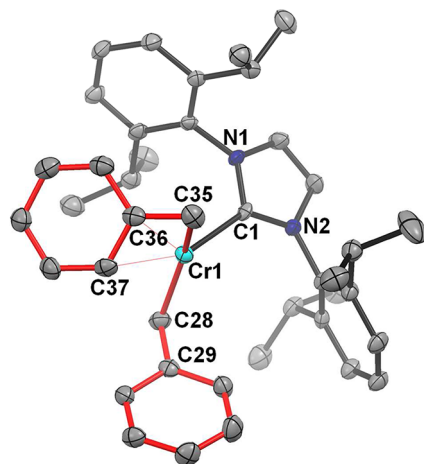


Figure 8. ORTEP of the Cr^{II} bis-benzyl complex **3**. Ellipsoids are at the 40% probability level. Hydrogen atoms are omitted for clarity. Selected distances (Å) and angles (deg): C1–Cr1 2.124(3), C28–Cr1 2.154(3); C35–Cr1 2.177(4), C36–Cr1 2.310(4), C37–Cr1 2.406(4), C28–Cr1–C35 153.80(14), C1–Cr1–C35 103.64(12), C1–Cr1–C28 100.66(12), C29–C28–Cr1 97.9(2), C36–C35–Cr1 76.6(2).

Table 1. Critical Angle Values (deg) in **2 and **3****

complex	PIMA excluded	PIMA included	experimental
2	103	93	93
3	87	75	77

[85.20(19)°, 88.85(19)°, 92.24(18)°, 98.6(2)°] observed in the newly redetermined X-ray structure of $[\text{ZrBz}_4]$ are also satisfactorily reproduced in the computed geometries of this complex in the gas phase and in the solvent shell (see Table S5, SI). With vanishing PIMA contribution, the deviation from sp^3 angle can mostly be attributed to standard and enhanced cation– π interactions owing to the presence of a +4 formal point charge. Independent studies published during the completion of our manuscript concluded on the flexibility of the benzyl critical angles in various crystallographic forms of $[\text{ZrBz}_4]$ but did not comment on its physical origin.¹⁶

CONCLUSION

Prompted by the structures of the novel Cr^{II} benzyl complexes **2**·THF and **3**, theoretical calculations led us to suggest that their unusual acute benzyl angles cannot solely be explained by the well-established orbital overlap and cation– π interactions, but are dictated to a considerable degree by intramolecular PIMA interactions. These manifest themselves when occupied metal d orbitals are suitably oriented to polarize the π system of the benzyl ring. Despite the fact that we are dealing here with cationic metal centers, the occupancy of their d orbitals is reminiscent of situations encountered in anion– π interactions.^{1–3} Whereas with empty metal d orbitals cation– π interactions are obviously enhanced, as in the 4d^0 complex $[\text{ZrBz}_4]$, PIMA interactions vanish. Although intermolecular crystal packing forces and steric effects are commonly invoked to explain structural distortions, they cannot account for the remarkable structures of **2**·THF and **3**. The emerging unifying view which includes PIMA interactions may have broader scope and applicability. Considering the energy range of PIMA interactions, we anticipate that these will provide a further

refinement toward the understanding of unusual molecular properties.

EXPERIMENTAL AND THEORETICAL SECTION

1. Synthesis and Characterization. 1.1. General Methods.

Elemental analyses were carried out by the microanalytical laboratory of London Metropolitan University. All manipulations were performed under nitrogen or argon in a Braun glovebox or using standard Schlenk techniques, unless stated otherwise. Solvents were dried using standard methods and distilled under nitrogen prior to use or passed through columns of activated alumina and subsequently purged with nitrogen or argon. The light petroleum used throughout had a bp 40–60 °C. The starting materials *N,N'*-diisopropylimidazol-2-ylidene and solutions of $[\text{Mg}(\text{benzyl})_2]$ and $[\text{Mg}(\text{benzyl})_2(\text{THF})_2]$ were prepared according to literature procedures.^{32,33} $[\text{CrCl}_2(\text{THF})_2]$ was prepared by continuous Soxhlet extraction of commercial anhydrous CrCl_2 with THF for 24–48 h under argon.

1.2. Synthesis of fac-Chromium Tri(benzyl)tris(tetrahydrofuran) (1). To a stirred solution of $[\text{Cr}(\text{acac})_3]$ (0.24 g, 0.7 mmol) in THF (5 mL) at –40 °C was added dropwise over a period of 5 min a precooled solution of freshly prepared $[\text{Mg}(\text{benzyl})_2]$ in ether (15 mL, 0.07 M, 1.05 mmol). After completion of the addition the purple suspension was stirred at –40 °C for 4 h. By the end of this period the reaction mixture was orange-brown. The reaction mixture was stored at –30 °C for 5–8 days, affording large orange-brown crystals, which were separated by syringing out the supernatant solution, washed with cold (–40 °C) petrol (2 × 5 mL), and dried with a stream of nitrogen. Drying under reduced pressure should be avoided because it leads to decomposition possibly due to loss of THF. The crystalline **1** is unstable at room temperature, completely collapsing into a brown oil over 30–40 min. Solutions of **1** in THF are noticeably unstable above –10 °C. Manipulations of the solid in the glovebox at room temperature can be carried out, but as quickly as possible (<5 min), with minor decomposition noticeable in this case too. Yield: 0.25 g. **1** was characterized by single-crystal X-ray diffraction as described below. Attempts to scale up the reaction (up to ca. 1.0 g of $[\text{Cr}(\text{acac})_3]$) resulted in reduced yields.

1.3. Synthesis of cis-Chromium Dibenzylbis(*N,N'*-diisopropylimidazol-2-ylidene) (2). To a cold (–78 °C) solution of **1** (0.25 g, 0.5 mmol) in THF (3 mL) was added a solution of *N,N'*-diisopropylimidazol-2-ylidene in toluene (4 mL, 0.28 M, 1.1 mmol). The solution color changed to red immediately. Cooling to –30 °C overnight gave air-sensitive, thermally unstable (>0 °C) dark orange crystals, which were characterized crystallographically; in the crystal the complex crystallized with one molecule of THF. Further efforts for spectroscopic or analytical characterization of **2** were hampered by the thermal instability.

1.4. Synthesis of Chromium Dibenzyl[*N,N'*-bis(2,6-diisopropylphenyl)imidazol-2-ylidene] (3). $[\text{CrCl}_2(\text{THF})_2]$ (0.25 g, 0.9 mmol) and *N,N'*-bis(2,6-diisopropyl phenyl)imidazol-2-ylidene (0.36 g, 0.9 mmol) were placed in a Schlenk tube in the glovebox. The tube was attached to the vacuum line and cooled to –78 °C by means of a dry ice acetone bath. At this temperature precooled THF (30 mL) and dioxane (2 mL) were added, followed by dropwise addition of a precooled solution of $[\text{Mg}(\text{benzyl})_2(\text{THF})_2]$ in THF (0.42 g, 1.2 mmol in 10 mL). The light green reaction mixture was allowed to warm to ca. 10 °C over a period of 16 h, giving a dark olive-green solution. After removal of the volatiles under reduced pressure, the residue was extracted with ether and filtered through Celite. Removal of the ether under reduced pressure gave the product as dark green-black crystalline material. X-ray quality crystals were obtained by cooling dilute ether or pentane solutions at 4 °C for 2 days. Yield: 0.42 g, ca. 75%. Anal. Found: C, 78.50; H, 7.95; N, 4.25. Calcd for $\text{C}_{41}\text{H}_{50}\text{CrN}_2$: C, 79.06; H, 8.09; N, 4.50. The ^1H NMR spectrum (C_6D_6) shows only broad features of low diagnostic value.

1.5. X-ray Crystallography. A summary of the crystal data, data collection, and refinement for complexes **1**, **2**·THF, **3**, and $[\text{ZrBz}_4]$ is given in Table S1 of the SI. All data sets were collected on a Enraf-Nonius Kappa CCD area detector diffractometer with an FR591 rotating anode (Mo $K\alpha$ radiation, $\lambda = 0.71073$ Å) and an Oxford

Cryosystems low-temperature device operating in ω scanning mode with ψ and ω scans to fill the Ewald sphere, except for **3**, which was collected on a Bruker APEX II DUO Kappa-CCD diffractometer equipped with an Oxford Cryosystem liquid N₂ device, using Mo K α radiation. The cell parameters were determined using the APEX2 software.³⁴ The programs used for control and integration were Collect, Scalepack, and Denzo.³⁵ All solutions and refinements were performed using the WinGX³⁶ package and all software packages within. All non-hydrogen atoms were refined using anisotropic thermal parameters, and hydrogen atoms were added using a riding model. The crystals were mounted on a glass fiber with silicon grease, from Fomblin vacuum oil. Crystals of the thermally unstable **1** and **2**·THF were quickly selected under a layer of Fomblin, which was kept at low temperatures (ca. -100 °C) by a stream of cold nitrogen. In **2**·THF, a disorder involved the cocrystallized THF molecule and one of the metalated benzyls. The solvent was disordered in three positions with no atom in common and was refined anisotropically with restrained geometrical and thermal parameters. The benzyl group was found disordered in two positions with no atom in common and was refined anisotropically with restrained geometrical and thermal parameters. A MULTISCAN absorption correction was applied for all structures.³⁷ CCDC crystallographic data (CCDC 868836 (**1**), 868837 (**2**·THF), 884835 (**3**), and 868838 ([ZrBz₄]) contain the supplementary crystallographic data for this paper, which can be obtained free of charge from the Cambridge Crystallographic Data Center via www.ccdc.cam.ac.uk/data_request/cif.

2. Computational Details. **2.1. Density Functional Theory Calculations.** DFT geometry optimizations were conducted for the different spin multiplicities $S = 0, 1,$ and 2 , starting from the X-ray data, first to track the packing effects. All calculations were performed using the Amsterdam Density Functional (ADF) program developed by Baerends and others.^{38,39} The numerical integration was performed using the procedure developed by te Velde et al.^{39g,h} The molecular orbitals (MOs) were expanded in an uncontracted set of Slater-type orbitals (STOs): TZP (no Gaussian functions are involved).³⁹ⁱ The basis set of triple- ζ quality was used for all atoms and augmented with one set of polarization functions on each atom, i.e., 2p on H, 3d on C and N, 4p on Cr, and 5p on Zr. The core shells of C and N (1s), Cr (up to 2p), and Zr (up to 3d) were treated by the frozen-(small)-core approximation.^{39c} An auxiliary set of s, p, d, f, and g STOs was used to fit the molecular density and to represent the Coulomb and exchange potentials accurately in each self-consistent field cycle.^{39j}

Equilibrium structures were optimized without any symmetry restrictions using analytical gradient techniques.^{39k} Because the BP86 density functional has been shown to be one of the three best GGA-DFT functionals (along with PBE and PW91), producing the high accuracy of optimized geometries using the ADF program package,⁴⁰ geometries and their relevant energies were calculated at the BP86 level of the generalized gradient approximation (GGA): exchange was described by Slater's $X\alpha$ potential^{39l} with self-consistent nonlocal corrections due to Becke,^{39m,n} and the electron correlation was treated in the Vosko–Wilk–Nusair (VWN) parametrization^{39o} with self-consistent nonlocal corrections due to Perdew^{39p} (BP86).^{39q} For the open-shell complexes, the spin-unrestricted formalism, U , was used. Grimme's dispersion correction to (U)BP86 of D3 generation^{25,29} (denoted as (U)BP86-D3) was implemented to evaluate the dependence of the studied complexes on dispersion.^{25–27,41} The dispersion-corrected (U)BP86 functional has been used efficiently to account for the possible London dispersion interactions, as was shown, for example, in ref 42. Scalar relativistic effects were accounted for using the zeroth-order regular approximation (ZORA).⁴³ Minimum energy geometries in the gas phase were verified to be equilibrium structures (no negative imaginary frequencies) through vibrational analysis.⁴⁴ With the goal to demonstrate that the gas-phase structures are independent of the presence of a homogeneous solvent medium used during crystallization, ZORA-(U)BP86(-D3)/TZP was combined with the conductor-like screening model (COSMO) of solvation with the solvent-excluding surface to define the cavities surrounding these structures.⁴⁵ THF ($\epsilon = 7.58$) was used as the solvent, and the atomic

radii were issued from the ADF program. Statistical thermal analysis was performed.

2.2. Ab Initio CASSCF/CASPT2 Calculations. It is known that some care must be taken in the presence of open shells. Indeed, the presence of quasi-degenerate configurations calls for explicitly correlated methods.⁴⁶ In this respect, complete active space self-consistent field (CASSCF) calculations allow one to generate a zeroth-order wave function starting from the exact Hamiltonian of the system. At this stage, all the physically relevant electronic configurations based on optimal MOs are explicitly taken into account. Subsequent second-order perturbation (CASPT2) calculations are then performed to include the important atomic-like contributions, which play a crucial role in the total energy determination. Let us stress that such calculations are particularly attractive since one can concentrate the numerical efforts on some part of the system and split the energy contribution taking advantage of the additive character of a perturbative treatment. This is precisely the strategy we used. Due to the presence of four electrons in the Cr 3d orbitals and six electrons of the π system, “mirror-glassing” CAS[10,10]SCF (10 electrons in 10 MOs) and subsequent CASPT2 were first carried out within each spin multiplicity. At this stage, the enlargement of the active space to include the mostly strongly antibonding $d_{x^2-y^2}$ orbital leaves the latter almost unoccupied. Such calculations were performed by varying one of the critical Cr–CH₂–C_{ipso} angles (CASPT2 potential energy curve), while the rest of the geometry was maintained identical to the X-ray one. Then, the active space was reduced down to a minimal CAS[4,4], and CAS[4,4]PT2 calculations were performed, (i) including all the inactive and virtual MOs and (ii) leaving out the 3 π -type and 3 π^* -type MOs localized on the aromatic ring. The difference between these two sets of calculations as a function of the critical angle corresponds to the contributions we would like to highlight. Besides, the structural impact of this contribution on the critical angle value can be followed by turning on this specific contribution. Physically, our inspection focuses on the instantaneous charge fluctuations on the aromatic ring responding to the electronic density localized on the Cr ion.

At the CAS[10,10] level of calculations, a leading open-shell character for all spin states ($S = 0, 1, 2$) was observed, meaning that the mostly d-like MOs are essentially singly occupied, and further quantitative analysis led to natural 3d-type orbitals with occupancy numbers in the range 0.999–1.001. The CAS[10,10]PT2 calculations established a $S = 2$ ground state, the other spin states being too high in energy (ca. 0.7 eV for $S = 1$) to compete with the $S = 2$ state.

All our calculations were performed using the MOLCAS 7.2 suite of programs.⁴⁷ In studies of weakly bound systems, one often encounters the problem known as basis set superposition error (BSSE). The Boys and Bernardi's counterpoise correction is a strategy to eliminate such an artificial effect.⁴⁸ This phenomenon has been recently examined in detail for single molecules, where the problem lies in the definition of the fragments to evaluate the counterpoise correction.⁴⁹ Another option is to increase the basis set quality since the error vanishes in the limit of a complete basis set. Therefore, particular care was taken in the definition of the interacting partners, and calculations were repeated by growing in a balanced way the atomic basis sets. Since our purpose was to concentrate the numerical effort on the π – π^* charge fluctuations, various extended ANO-RCC basis sets were used for the aromatic ring, the *ipso* carbon, and the chromium ion.⁵⁰

Calculations for the $S = 0, 1,$ and 2 spin states were performed successively using (i) double- ζ + polarization (DZP, 3s2p1d and 5s3p2d1f for C and Cr, respectively), (ii) triple- ζ + polarization (TZP, 4s3p2d1f and 6s4p3d2f1g for C and Cr, respectively), and ultimately (iii) quadruple- ζ + polarization (QZP, 5s4p3d2f and 7s5p4d3f2g for C and Cr, respectively) along with a 2s1p contraction for the hydrogen atoms of the aromatic ring. The three other nearest neighbor C atoms of the Cr coordination sphere hold a DZP basis set, while the rest of the atoms of **2** and **3** are depicted using a DZ basis set. From this numerical inspection, the convergence of the calculated CASPT2 energy differences with the basis set improvement is reached at the TZP level. Indeed, the calculated energy differences vary by less than 2 kJ/mol (e.g., 5% for the PIMA contribution) when the basis set is

changed from TZP to QZP. In addition, the positions of the minima of the potential energy curves are modified by less than 2°, a value that is well below the experimentally observed critical angle value variations.

In light of this numerical inspection performed on the Cr^{II} complex 2, a TZP basis set quality was used for the Zr^{IV} compound [ZrBz₄]. The main difference lies in the empty character of the 4d orbitals of the formally Zr⁴⁺ ion.

■ ASSOCIATED CONTENT

● Supporting Information

Experimental details, crystallographic data (CCDC 868836 (1), 868837 (2-THF), 884835 (3), and 868838 ([ZrBz₄]), and details of calculations. This material is available free of charge via the Internet at <http://pubs.acs.org>.

■ AUTHOR INFORMATION

Corresponding Author

*E-mail: danopoulos@unistra.fr (A.A.D.), vrobert@unistra.fr (V.R.), braunstein@unistra.fr (P.B.).

Notes

The authors declare no competing financial interest.

■ ACKNOWLEDGMENTS

We thank the CNRS, the Université de Strasbourg (UdS), the Ministère de l'Enseignement Supérieur et de la Recherche (Paris), the International Center for Frontier Research in Chemistry, Strasbourg (ucFRC, www.icfrc.fr), and the LabEx "Chemistry of Complex Systems". A.A.D. is grateful to the Région Alsace, the Département du Bas-Rhin, and the Communauté Urbaine de Strasbourg, for the award of a Gutenberg Excellence Chair (2010–2011), and to the University of Strasbourg Institute for Advanced Study for a Fellowship (2013–2014). K.Y.M. is grateful to the Deutsche Forschungsgemeinschaft (DFG) and the Gutenberg funding for postdoctoral fellowships. S.C.-G. thanks Sasol Technology UK for funding. We thank the UdS High-Performance Computing Center for the provision of computational facilities and the Service de Radiocristallographie (Institut de Chimie, Strasbourg) for assistance with the crystallography. We are grateful to Profs. P. Chen, J. C. Green, S. Grimme, and R. Hoffmann for their valuable input and to Dr. G. Pilet, M. Vérot, and F. Houis for producing the artwork.

■ REFERENCES

- (1) Salonen, L. M.; Ellermann, M.; Diederich, F. *Angew. Chem., Int. Ed.* **2011**, *50*, 4808–4842.
- (2) Beer, P. D.; Gale, P. A. *Angew. Chem., Int. Ed.* **2001**, *40*, 486–516.
- (3) Schottel, B. L.; Chifotides, H. T.; Dunbar, K. R. *Chem. Soc. Rev.* **2008**, *37*, 68–83.
- (4) Sinnokrot, M. O.; Sherrill, C. D. *J. Phys. Chem. A* **2006**, *110*, 10656–10668.
- (5) Bhandari, G.; Kim, Y.; McFarland, J. M.; Rheingold, A. L.; Theopold, K. H. *Organometallics* **1995**, *14*, 738–745.
- (6) Agapie, T.; Day, M. W.; Henling, L. M.; Labinger, J. A.; Bercaw, J. E. *Organometallics* **2006**, *25*, 2733–2742.
- (7) van Leeuwen, P. W. N. M.; Clément, N. D.; Tschan, M. J. L. *Coord. Chem. Rev.* **2011**, *255*, 1499–1517.
- (8) (a) Hogan, J. P.; Banks, R. L. Phillips Petroleum Co., Belg. Pat. 530617, 1955; U.S. Pat. 2825721, 1958. (b) Hogan, J. P. *J. Polym. Sci.* **1970**, *8*, 2637–2652. (c) Karapinka, G. L. U.S. Pat. 3709853, 1973. (d) Karol, F. J.; Karapinka, G. L.; Wu, C.; Dow, A. W.; Johnson, R. N.; Garrick, W. L. *J. Polym. Sci.* **1972**, *10*, 2621–2637.
- (9) Cazin, S. J. C. *N-Heterocyclic Carbenes in Transition Metal Catalysis and Organocatalysis*; Springer Verlag, 2010.
- (10) Enders, D.; Niemeier, O.; Henseler, A. *Chem. Rev.* **2007**, *107*, 5606–5655.
- (11) Hahn, F. E.; Jahnke, M. C. *Angew. Chem., Int. Ed.* **2008**, *47*, 3122–3172.
- (12) Kim, S.-K.; Kim, T.-J.; Chung, J.-H.; Hahn, T.-K.; Chae, S.-S.; Lee, H.-S.; Cheong, M.; Kang, S. O. *Organometallics* **2010**, *29*, 5805–5811.
- (13) Yang, Y.; Liu, Z.; Zhong, L.; Qiu, P.; Dong, Q.; Cheng, R.; Vanderbilt, J.; Liu, B. *Organometallics* **2011**, *30*, 5297–5302.
- (14) McDyre, L.; Carter, E.; Cavell, K. J.; Murphy, D. M.; Platts, J. A.; Sampford, K.; Ward, B. D.; Gabrielli, W. F.; Hanton, M. J.; Smith, D. M. *Organometallics* **2011**, *30*, 4505–4508.
- (15) See, for example: (a) Legzdins, P.; Jones, R. H.; Phillips, E. C.; Yee, V. C.; Trotter, J.; Einstein, F. W. B. *Organometallics* **1991**, *10*, 986. (b) Scholz, J.; Rehbaum, F.; Thiele, K. H.; Goddard, R.; Betz, P.; Kruger, C. J. *Organomet. Chem.* **1993**, *443*, 93. (c) Pellecchia, C.; Immirzi, A.; Pappalardo, D.; Peluso, A. *Organometallics* **1994**, *13*, 3773.
- (16) Rong, Y.; Al-Harbi, A.; Parkin, G. *Organometallics* **2012**, *31*, 8208–8217.
- (17) Köhn, R. D.; Kociok-Köhn, G.; Haufe, M. J. *Organomet. Chem.* **1995**, *501*, 303–307.
- (18) Schrock, R. R.; Parshall, G. W. *Chem. Rev.* **1976**, *76*, 243–268.
- (19) Zucchini, U.; Albizzati, E.; Giannini, U. *J. Organomet. Chem.* **1971**, *26*, 357–372.
- (20) Chen, E. Y. X.; Rodriguez-Delgado, A. In *Comprehensive Organometallic Chemistry III*; Vol. 4 (Bochmann, M., Vol. Ed.; Crabtree, R. H.; Mingos, D. M. P., Chief Eds.), Elsevier, 2007; pp 759–1004.
- (21) (a) Coles, M. P.; Dalby, C. I.; Gibson, V. C.; Clegg, W.; Elsegood, M. R. J. *Chem. Commun.* **1995**, 1709. (b) Siemeling, U.; Kölling, L.; Stammler, A.; Stammler, H.-G.; Kaminski, E.; Fink, G. *Chem. Commun.* **2000**, 1177–1178.
- (22) Jandciu, E. W.; Kuzelka, J.; Legzdins, P.; Rettig, S. J.; Smith, K. M. *Organometallics* **1999**, *18*, 1994–2004.
- (23) (a) Bei, X.; Swenson, D. C.; Jordan, R. F. *Organometallics* **1997**, *16*, 3282–3302. (b) Giesbrecht, G. R.; Whitener, G. D.; Arnold, J. *Organometallics* **2000**, *19*, 2809–2812.
- (24) Zukerman-Schpector, J.; Otero-de-la-Roza, A.; Luaña, V.; Tiekink, E. R. T. *Chem. Commun.* **2011**, *47*, 7608–7610.
- (25) Grimme, S. *J. Comput. Chem.* **2006**, *27*, 1787–1799.
- (26) Grimme, S.; Antony, J.; Schwabe, T.; Mück-Lichtenfeld, C. *Org. Biomol. Chem.* **2007**, *5*, 741.
- (27) Grimme, S.; Hünerbein, R.; Ehrlich, S. *ChemPhysChem.* **2011**, *12*, 1258.
- (28) Grimme, S. *Chem.—Eur. J.* **2012**, *18*, 9955–9964.
- (29) Grimme, S.; Anthony, J.; Ehrlich, S.; Krieg, H. *J. Chem. Phys.* **2010**, *132*, 154104.
- (30) Kepenekian, M.; Le Guennic, B.; Awaga, K.; Robert, V. *Phys. Chem. Chem. Phys.* **2009**, *11*, 6066–6071.
- (31) Viciu, M. S.; Navarro, O.; Germaneau, R. F.; Kelly, R. A., III; Sommer, W.; Marion, N.; Stevens, E. D.; Cavallo, L.; Nolan, S. P. *Organometallics* **2004**, *23*, 1629–1635.
- (32) Burling, S.; Paine, B. M.; Nama, D.; Brown, V. S.; Mahon, M. F.; Prior, T. J.; Pregosin, P. S.; Whittlesey, M. K.; Williams, J. M. J. *J. Am. Chem. Soc.* **2007**, *129*, 1987.
- (33) Wagner, B. O.; Hammond, G. J. *Organomet. Chem.* **1975**, *85*, 1.
- (34) APEX2; BrukerAXS Inc: Madison, WI, USA, 2006.
- (35) Hooft, R. COLLECT; Nonius BV, 1997–2000. Otwinoski, Z.; Minor, W. SCALEPACK, DENZO. *Methods Enzymol.* **1997**, *276*, 307.
- (36) Farrugia, L. J. *J. Appl. Crystallogr.* **1999**, *32*, 83.
- (37) Blessing, R. H. *Acta Crystallogr., Sect. A* **1995**, *51*, 33.
- (38) Baerends, E. J.; Autschbach, J.; Bérces, A.; Bo, C.; Boerrigter, P. M.; Cavallo, L.; Chong, D. P.; Deng, L.; Dickson, R. M.; Ellis, D. E.; Fan, L.; Fischer, T. H.; Fonseca Guerra, C.; van Gisbergen, S. J. A.; Groeneveld, J. A.; Gritsenko, O. V.; Grüning, M.; Harris, F. E.; van den Hoek, P.; Jacobsen, H.; van Kessel, G.; Kootstra, F.; van Lenthe, E.; McCormack, D. A.; Osinga, V. P.; Patchkovskii, S.; Philipsen, P. H. T.; Post, D.; Pye, C. C.; Ravenek, W.; Ros, P.; Schipper, P. R. T.; Schreckenbach, G.; Snijders, J. G.; Solà, M.; Swart, M.; Swerhone, D.;

te Velde, G.; Vernooijs, P.; Versluis, L.; Visser, O.; van Wezenbeek, E.; Wiesenekker, G.; Wolff, S. K.; Woo, T. K.; Ziegler, T. *ADF2010.01*; 2010, SCM, Theoretical Chemistry, Vrije Universiteit: Amsterdam, The Netherlands, <http://www.scm.com>.

(39) (a) te Velde, G.; Bickelhaupt, F. M.; Baerends, E. J.; Fonseca Guerra, C.; van Gisbergen, S. J. A.; Snijders, J. G.; Ziegler, T. *J. Comput. Chem.* **2001**, *22*, 931. (b) Fonseca Guerra, C.; Visser, O.; Snijders, J. G.; te Velde, G.; Baerends, E. J. In *Methods and Techniques for Computational Chemistry*; Clementi, E.; Corongiu, G., Eds.; STEF: Cagliari, 1995; pp 305–395. (c) Baerends, E. J.; Ellis, D. E.; Ros, P. *Chem. Phys.* **1973**, *2*, 41. (d) Baerends, E. J.; Ros, P. *Chem. Phys.* **1975**, *8*, 412. (e) Baerends, E. J.; Ros, P. *Int. J. Quantum Chem. Symp.* **1978**, *12*, 169. (f) Fonseca Guerra, C.; Snijders, J. G.; te Velde, G.; Baerends, E. J. *Theor. Chem. Acc.* **1998**, *99*, 391. (g) Boerrigter, P. M.; te Velde, G.; Baerends, E. J. *Int. J. Quantum Chem.* **1988**, *33*, 87. (h) te Velde, G.; Baerends, E. J. *J. Comput. Phys.* **1992**, *99*, 84. (i) Snijders, G.; Vernooijs, P.; Baerends, E. J. *At. Nucl. Data Tables* **1981**, *26*, 483. (j) Krijn, J.; Baerends, E. J. *Fit-Functions in the HFS-Method; Internal Report (in Dutch)*; Vrije Universiteit: Amsterdam, 1984. (k) Versluis, L.; Ziegler, T. *J. Chem. Phys.* **1988**, *88*, 322. (l) Slater, J. C. *Quantum Theory of Molecules and Solids*, Vol. 4; McGraw-Hill: New York, 1974. (m) Becke, A. D. *J. Chem. Phys.* **1986**, *84*, 4524. (n) Becke, A. D. *Phys. Rev. A* **1988**, *38*, 3098. (o) Vosko, S. H.; Wilk, L.; Nusair, M. *Can. J. Phys.* **1980**, *58*, 1200. (p) Perdew, J. P. *Phys. Rev. B* **1986**, *33*, 8822; Erratum *Phys. Rev. B* **1986**, *34*, 7406. (q) Fan, L.; Ziegler, T. *J. Chem. Phys.* **1991**, *94*, 6057.

(40) Swart, M.; Snijders, J. G. *Theor. Chem. Acc.* **2003**, *110*, 34; Erratum *Theor. Chem. Acc.* **2004**, *111*, 56.

(41) (a) Grimme, S. *J. Comput. Chem.* **2004**, *25*, 1463. (b) Siegbahn, P. E. M.; Blomberg, M. R. A.; Chen, S.-L. *J. Chem. Theory Comput.* **2010**, *6*, 2040.

(42) See, for example: (a) Ruiz, J. M.; Fonseca Guerra, C.; Bickelhaupt, F. M. *J. Phys. Chem. A* **2011**, *115*, 8310. (b) Banerjee, A.; Raad, F. S.; Vankova, N.; Bassil, B. S.; Heine, T.; Kortz, U. *Inorg. Chem.* **2011**, *50*, 11667. (c) Ames, W.; Pantazis, D. A.; Krewald, V.; Cox, N.; Messinger, J.; Lubitz, W.; Neese, F. *J. Am. Chem. Soc.* **2011**, *133*, 19743.

(43) van Lenthe, E.; Baerends, E. J.; Snijders, J. G. *J. Chem. Phys.* **1994**, *101*, 9783.

(44) (a) Bérces, A.; Dickson, R. M.; Fan, L.; Jacobsen, H.; Swerhone, D.; Ziegler, T. *Comput. Phys. Commun.* **1997**, *100*, 247. (b) Jacobsen, H.; Bérces, A.; Swerhone, D.; Ziegler, T. *Comput. Phys. Commun.* **1997**, *100*, 263. (c) Wolff, S. K. *Int. J. Quantum Chem.* **2005**, *104*, 645.

(45) (a) Klamt, A.; Schüürmann, G. *J. Chem. Soc., Perkin Trans.* **1993**, *2*, 799. (b) Klamt, A. *J. Phys. Chem.* **1995**, *99*, 2224. (c) Klamt, A.; Jones, V. *J. Chem. Phys.* **1996**, *105*, 9972.

(46) (a) Banse, F.; Girerd, J.-J.; Robert, V. *Eur. J. Inorg. Chem.* **2008**, 4786–4791. (b) Kepenekian, M.; Vetere, V.; Calborean, A.; Le Guennic, B.; Maldivi, P.; Robert, V. *Chem.—Eur. J.* **2011**, *17*, 12045–12050. (c) Kepenekian, M.; Vetere, V.; Calborean, A.; Le Guennic, B.; Maldivi, P.; Robert, V. *J. Chem. Theor. Comput.* **2011**, *7*, 3532–3539.

(47) MOLCAS The Next Generation. *J. Comput. Chem.* **2010**, *31*, 224–247.

(48) Boys, S. F.; Bernardi, F. *Mol. Phys.* **1970**, *19*, 553.

(49) Asturiol, D.; Duran, M.; Salvador, P. *J. Chem. Phys.* **2008**, *128*, 144108.

(50) Roos, B. O.; Lindh, R.; Malmqvist, P.-Å.; Veryazov, V.; Widmark, P.-O. *J. Phys. Chem. A* **2005**, *108*, 2851.